Recent Progress in Self-Lubricating Ceramic Composites

8

Guangyong Wu, Chonghai Xu, Guangchun Xiao, and Mingdong Yi

Contents

Abstract

Structural ceramic composites have received increasing attention over the past few decades for their potential applications in various fields. Lubrication is usually required for moving ceramic parts because of their high coefficient of friction under dry sliding conditions. Self-lubricating ceramic composites have been applied in severe operating conditions where conventional lubrication method, such as liquid lubrication, is unavailable. The solid lubricants added in

G. Wu
School of Mechanical Engineering, Shandong University, Jinan, China
e-mail: gywu168@sina.com

C. Xu (✉)
School of Mechanical Engineering, Shandong University, Jinan, China

School of Mechanical and Automotive Engineering, Qilu University of Technology, Jinan, China

Key Laboratory of Advanced Manufacturing and Measurement and Control Technology for Light Industry in Universities of Shandong, Qilu University of Technology, Jinan, China
e-mail: xch@qlu.edu.cn

G. Xiao · M. Yi
School of Mechanical and Automotive Engineering, Qilu University of Technology, Jinan, China

Key Laboratory of Advanced Manufacturing and Measurement and Control Technology for Light Industry in Universities of Shandong, Qilu University of Technology, Jinan, China

P. L. Menezes et al. (eds.), *Self-Lubricating Composites*,
https://doi.org/10.1007/978-3-662-64243-6_8

self-lubricating ceramic composites can reduce the coefficient of friction. However, they decrease mechanical properties and then weaken antiwear property of the ceramic composites, which consequently restricts self-lubricating ceramic composites' application scope. Therefore, there is a contradiction between the antifriction and antiwear properties of self-lubricating ceramic composites and many efforts from researchers have been devoted to resolve it. In this chapter, two new types of self-lubricating ceramic composites were elaborated. Graded self-lubricating ceramic composites were developed by adopting the design concept of functionally graded materials (FGMs). Their characteristics are that the solid lubricant content decreases with a gradient from the surface to the center and thermal residual compressive stresses exist in the surface after the sintering process. The gradient distribution of solid lubricant and the thermal residual compressive stresses are used to improve the mechanical properties of the ceramic composites. Another new type of self-lubricating ceramic composites is those with the addition of coated solid lubricants. The solid lubricant powders are firstly coated by metal or metallic oxide, etc., to form core-shell structured composite powders and then mixed with the ceramic matrix powders to prepare self-lubricating ceramic composites by sintering. The shell substance is used to protect the solid lubricant core from reacting with the ceramic matrix during the sintering process and promote the relative density of the ceramic composites. The two new types of self-lubricating ceramic composites showed superior mechanical properties and tribological properties to the traditional self-lubricating ceramic composites.

8.1 Introduction

Nowadays, structural ceramic composites have been paid attention increasingly for their distinctive properties, such as high hardness, high wear resistance, high-temperature resistance, and good chemical inertness [1]. They have been widely used for many applications, for instance, cutting tools, bearing parts, valve seats, etc. However, the friction coefficient of moving ceramic parts, especially of those made of alumina based ceramic composites, is relatively high [2]. Higher friction coefficient causes more cost and energy waste. The traditional oil or grease lubrication not only leads to environmental pollution, but also loses efficacy under harsh conditions, such as elevated temperature. Besides, due to poor thermal shock resistance of ceramic composites, inappropriate cooling will cause hot cracks and breakage. Therefore, development and application of ceramic composites with self-lubricating function is an effective and eco-friendly solution to improve the antifriction properties.

So far there are three main methods to make ceramic composites possess self-lubricating function: (1) make use of tribochemical reaction under high working temperature to get in situ formed tribofilm with lubricating function on the surface of ceramic composites, (2) adopt coating, impregnation, or implantation technologies

to enable the surface of ceramic composites to have lubricating function, and (3) fabricate self-lubricating ceramic composites which contain solid lubricants. Compared with the other two methods, the third one can make ceramic composites possess self-lubricating function during their whole service life because there are always solid lubricants in the composites. Besides, it can make the self-lubricating function be available in a wide working temperature range.

The traditional self-lubricating ceramic composites are homogeneous materials with the addition of pristine solid lubricants. Many researches revealed that the added solid lubricants can produce both positive and negative effects on properties of ceramic composites [3, 4]. On the one hand, the solid lubricant can reduce the friction coefficient by forming a tribofilm in the working areas. However, on the other hand, the dispersed solid lubricants can cause a decline in mechanical properties of the ceramic matrix, especially the hardness and fracture toughness, and thus reduce the wear resistance of the ceramic composite [5]. Thus, the traditional self-lubricating ceramic composites are not available to possess rational combination of antifriction and antiwear properties, which consequently restricts their application scope. It is urgent and significant to develop new type of self-lubricating ceramic composites.

In the past few years, we proposed and developed two new types of self-lubricating ceramic composites by modifying the traditional self-lubricating ceramic composites at macroscopic and microscopic level, respectively. The first type is graded self-lubricating ceramic composites [6–8]. It is macrostructural modification to the traditional self-lubricating ceramic composites. The second type is self-lubricating ceramic composites with the addition of metal coated solid lubricants [9]. It is microstructural modification to the traditional self-lubricating ceramic composites.

This chapter introduced the two new types of self-lubricating ceramic composites. Their microstructures, mechanical properties, and tribological properties were studied in detail.

8.2 Graded Self-Lubricating Ceramic Composites

Graded self-lubricating ceramic composites were proposed in terms of macrostructural modification to the traditional self-lubricating ceramic composites. This new type of self-lubricating ceramic composite is characterized by gradually decreasing distribution of solid lubricants from the composite's working surface to its interior and the residual compressive stresses existing in the working surface. There are two design criteria for the graded self-lubricating ceramic composites. Firstly, the solid lubricants should be gradually reduced from the working surface to the interior. Secondly, the thermal expansion coefficient of the composite should gradually increase from the working surface to the inside in order to form residual compressive stresses in the working surface after the sintering process [10].

CaF_2 is well known as a high-temperature solid lubricant and Al_2O_3/(W,Ti)C ceramic is a kind of widely used ceramic material, thus Al_2O_3/(W,Ti)C and CaF_2 were chosen to be the matrix material and solid lubricant, respectively. The starting

Table 8.1 Physical properties of the starting powders

Starting powder	Density ρ ($g{\cdot}cm^{-3}$)	Young's modulus E (GPa)	Poisson's ratio ν	Thermal expansion coefficient α ($\times 10^{-6}\ K^{-1}$)	Thermal conductivity k ($W{\cdot}m^{-1}\ K^{-1}$)
α-Al_2O_3	3.99	380	0.26	8.5	40.37
(W,Ti)C	9.56	550	0.194	5.8	26.74
CaF_2	3.18	75.8	0.26	18.85	9.71

powders were commercial Al_2O_3, (W,Ti)C, and CaF_2 and their physical properties are listed in Table 8.1.

Al_2O_3/(W,Ti)C/CaF_2 graded self-lubricating ceramic composite was designed in disk shape with its compositional distribution changing along the thickness direction. In order that the top and bottom surfaces of the composite can be used as work surfaces with the same self-lubricating performance, a symmetrically laminated structure with seven layers was adopted. Because the graded self-lubricating ceramic composite consists of three components which are Al_2O_3, (W,Ti)C, and CaF_2, a multicomponent gradient distribution model was proposed [7, 8]. The distribution model uses symmetrical power-law functions containing two compositional distribution exponents n_1 and n_2 which are for CaF_2 and (W,Ti)C, respectively.

The geometry model of Al_2O_3/(W,Ti)C/CaF_2 graded self-lubricating ceramic composite is a cylinder in a Cartesian coordinate system. The cylinder's bottom surface is in the X-Y plane and its axis coincides with the Z axis. The diameter and height of the cylinder are D and H, respectively. Because of their very small amounts, pores and sintering additives are not taken into account in the multicomponent distribution model. By regarding α-Al_2O_3 and (W,Ti)C as a matrix component, the volume fraction of CaF_2 in Al_2O_3/(W,Ti)C/CaF_2 material along the thickness of the material is given as:

$$V_{CaF_2} = f_1(\xi) = \begin{cases} \left(f_1^{CF} - f_0^{CF}\right)\left[\frac{0.5-\xi}{0.5}\right]^{n_1} + f_0^{CF} & 0 \le \xi \le 0.5 \\ \left(f_1^{CF} - f_0^{CF}\right)\left[\frac{\xi-0.5}{0.5}\right]^{n_1} + f_0^{CF} & 0.5 \le \xi \le 1 \end{cases} \tag{8.1}$$

Where ξ is the ratio of arbitrary coordinate value along the thickness direction (z) to the total thickness of the Al_2O_3/(W,Ti)C/CaF_2 material (H), i.e., z/H, and the range of ξ is [0,1]; ${f_1}^{CF}$ and ${f_0}^{CF}$ are volume fractions of CaF_2 in the Al_2O_3/(W,Ti)C/CaF_2 material of the surface layers and the middle layer, respectively; n_1 is the compositional distribution exponent for CaF_2 distributing in the Al_2O_3/(W,Ti)C/CaF_2 material.

Then the composition profile of the Al_2O_3/(W,Ti)C matrix component is determined as $V_{Al_2O_3/(W,Ti)C} = 1 - V_{CaF_2}$.The volume fraction of (W,Ti)C in the matrix along the thickness of the Al_2O_3/(W,Ti)C/CaF_2 material is given as:

$$V^*_{(W,Ti)C} = f_2(\xi) = \begin{cases} \left(f_1^{WT} - f_0^{WT}\right)\left[\frac{0.5-\xi}{0.5}\right]^{n_2} + f_0^{WT} & 0 \le \xi \le 0.5 \\ \left(f_1^{WT} - f_0^{WT}\right)\left[\frac{\xi-0.5}{0.5}\right]^{n_2} + f_0^{WT} & 0.5 \le \xi \le 1 \end{cases} \tag{8.2}$$

Where ξ is the same as in Eq. (8.1); ${f_1}^{WT}$ and ${f_0}^{WT}$ are volume fractions of (W,Ti)C in the Al_2O_3/(W,Ti)C matrixes of the surface layers and the middle layer, respectively; n_2 is the compositional distribution exponent for (W,Ti)C distributing in the Al_2O_3/(W,Ti)C matrix.

The volume fraction of (W,Ti)C in Al_2O_3/(W,Ti)C/CaF_2 material along the thickness of the material should be given as:

$$V_{(W,Ti)C} = (1 - f_1(\xi))f_2(\xi) \tag{8.3}$$

And the volume fraction of Al_2O_3 in Al_2O_3/(W,Ti)C/CaF_2 material along the thickness of the material should be given as:

$$V_{Al_2O_3} = (1 - f_1(\xi))(1 - f_2(\xi)) = 1 - V_{CaF_2} - V_{(W,Ti)C} \tag{8.4}$$

The combinations of nonnegative values of n_1 and n_2 can determine the compositional distributions of Al_2O_3/(W,Ti)C/CaF_2 material and then its gradients of microstructure as well as properties. According to values of n_1 and n_2, Al_2O_3/(W,Ti)C/CaF_2 material can be categorized into five general types:

(a) $n_1 = n_2 = 0$. Volume fraction of CaF_2 in the whole material and volume fraction of (W,Ti)C in the matrix are constant to form homogeneous material.
(b) $n_1 = 0$, $n_2 \neq 0$. Volume fraction of CaF_2 in the whole material is constant and volume fraction of (W,Ti)C in the matrix is varying to form the first kind of graded material.
(c) $n_1 \neq 0$, $n_2 = 0$. Volume fraction of CaF_2 in the whole material is varying and volume fraction of (W,Ti)C in the matrix is constant to form the second kind of graded material.
(d) $n_1 = n_2 \neq 0$. Volume fraction of CaF_2 in the whole material and volume fraction of (W,Ti)C in the matrix are varying with the same rate to form the third kind of graded material.
(e) $n_1 \neq n_2 \neq 0$. Volume fraction of CaF_2 in the whole material and volume fraction of (W,Ti)C in the matrix are varying with different rates to form the fourth kind of graded material.

In order to conform the two design criteria and use a simpler structure, the compositional distribution exponents were chosen to be $n_1 = n_2 = 2.0$. The detailed design procedure was presented in [7]. Table 8.2 lists the compositions of each layer and their physical properties which were calculated by the formulae in [10].

The Al_2O_3/(W,Ti)C/CaF_2 graded self-lubricating ceramic composite was prepared using a layer stacking method and powder metallurgical process. The detailed preparation process and measurement method of mechanical properties were described in [7]. An Al_2O_3/(W,Ti)C/CaF_2 homogeneous self-lubricating ceramic composite was also made from the same ingredients with the surface layers of the graded composite. Phase identification was made by X-ray diffraction (XRD) using an X-ray diffractometer (Bruker D8 ADVANCE). XRD patterns were recorded from

Table 8.2 Compositions and physical properties of graded layers

Layer number	Content of CaF_2 (Vol. %)	Volume ratio of (W,Ti)C: α-Al_2O_3 in matrix (Vol %)	Young's modulus E (GPa)	Poisson's ratio ν	Thermal expansion coefficient α ($\times 10^{-6}$ K^{-1})	Thermal conductivity k ($W \cdot m^{-1}$ K^{-1})
4th	0	30:70	424.710	0.242	7.660	35.156
3rd;5th	3.3	40:60	420.602	0.235	7.516	32.275
2nd;6th	6.7	50:50	415.416	0.229	7.386	29.643
1st;7th	10	60:40	410.367	0.223	7.262	27.303

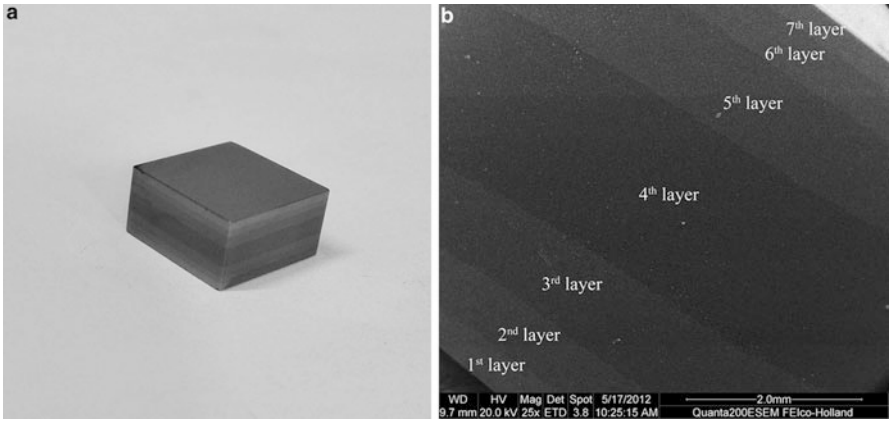

Fig. 8.1 (**a**) Optical photograph and (**b**) SEM micrograph of Al_2O_3/(W,Ti)C/CaF_2 graded composite

20° to 80° with a step of 0.02° under the condition of 40 kV and 20 mA. The componential distribution of Al_2O_3/(W,Ti)C/CaF_2 graded composite was analyzed by line scanning technique with energy dispersive spectrometer (EDS, Oxford INCAx-act). The microstructures were observed on polished cross section and fracture surfaces by environmental scanning electron microscope (ESEM, model FEI-quanta 200).

Optical photograph of Al_2O_3/(W,Ti)C/CaF_2 graded ceramic composite is shown in Fig. 8.1a. It can be seen that the layers are perpendicular to the thickness direction. SEM micrograph of the cross section surface is shown in Fig. 8.1b. A symmetrical seven-layer structure can be easily observed. The higher the (W,Ti)C content of a layer is, the brighter the layer looks like. The layer interfaces are straight and parallel to each other, which is in accord with the design objective.

The microstructural changes which agree with the gradient variation of the components are shown in Fig. 8.2. The darker phase in the micrographs is identified by EDS to be Al_2O_3 and the brighter phase is (W,Ti)C and CaF_2. From the first layer (surface layer) to the fourth layer (middle layer), because the content of Al_2O_3

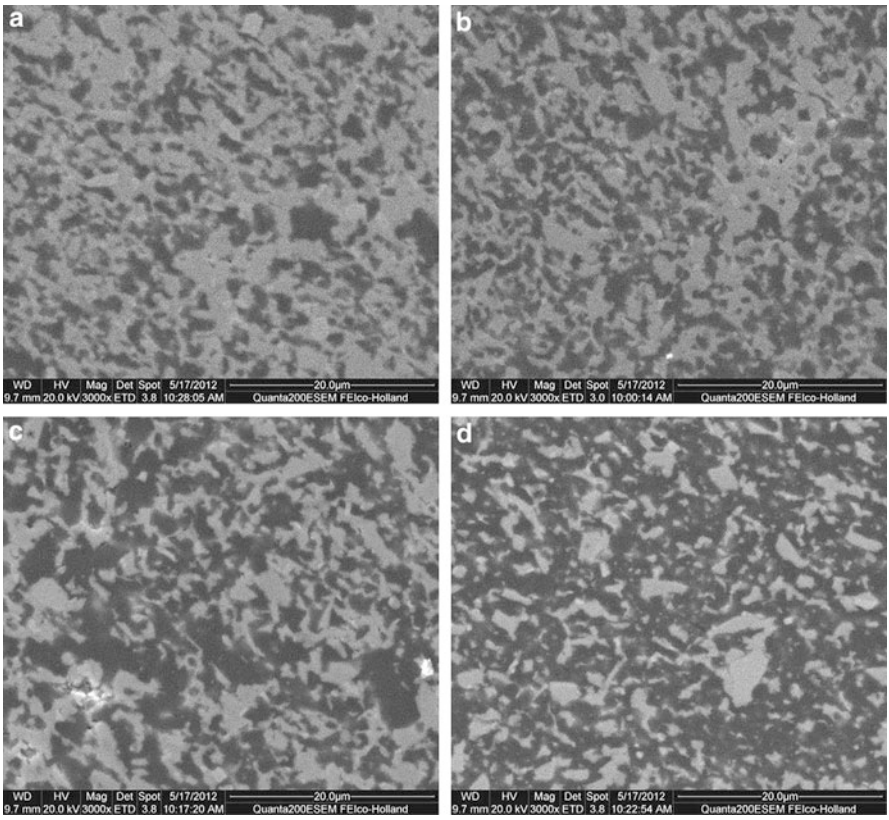

Fig. 8.2 SEM micrographs of the polished surface of Al_2O_3/(W,Ti)C/CaF_2 graded composite: (**a**) the 1st layer, (**b**) the 2nd layer, (**c**) the 3rd layer, and (**d**) the 4th layer

increases meanwhile the content of (W,Ti)C and CaF_2 decreases layer by layer, the proportion of darker areas in the micrographs increases and brighter areas follow the opposite variation trend. Furthermore, the phases in each layer are uniformly distributed and form relatively dense microstructures.

The SEM micrographs of the fractured surface of the Al_2O_3/(W,Ti)C/CaF_2 graded self-lubricating ceramic composite are shown in Fig. 8.3. It can be seen that each phase in the different layers has small and uniform grains. The cavities that are left after grains were pulled out can be observed. This sign indicates typical intergranularc fracture. The wavy or stepped features formed after grains were fractured can also be observed, which indicates typical transgranular fracture. Therefore, mixed intergranular fracture and transgranular fracture are fracture modes of the graded self-lubricating ceramic composite.

Figure 8.4 illustrates XRD pattern of surface layer of the Al_2O_3/(W,Ti)C/CaF_2 graded self-lubricating ceramic composite. It can be seen that Al_2O_3, (W,Ti)C, and CaF_2 phases well exist in the composite.

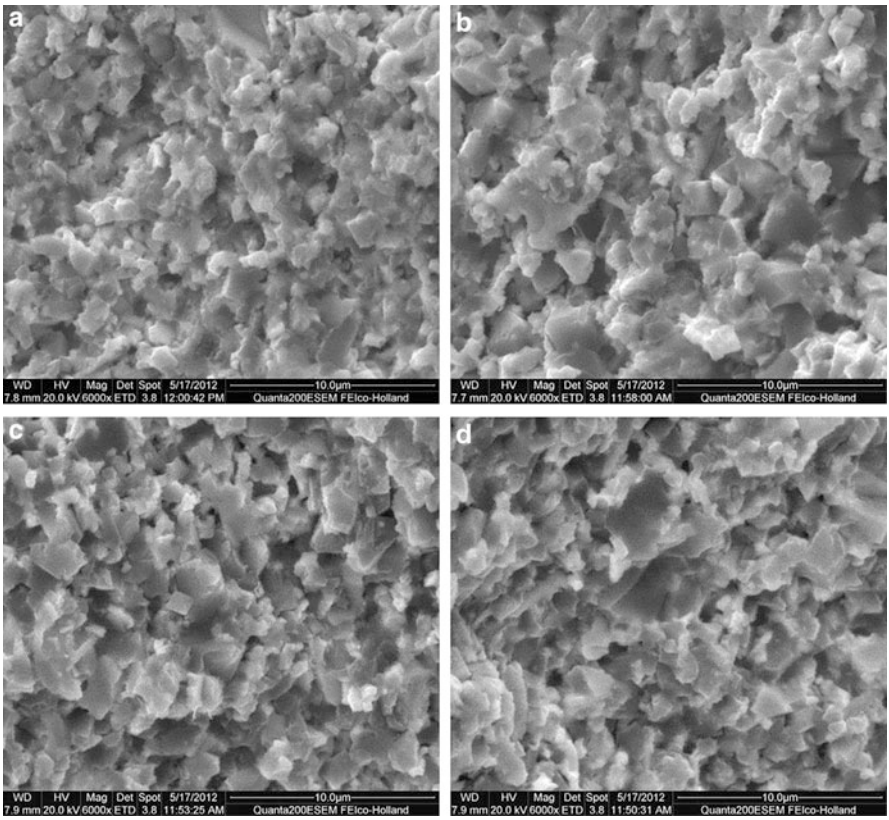

Fig. 8.3 SEM micrographs of the fractured surface of Al_2O_3/(W,Ti)C/CaF_2 graded composite: (**a**) the 1st layer, (**b**) the 2nd layer, (**c**) the 3rd layer, and (**d**) the 4th layer

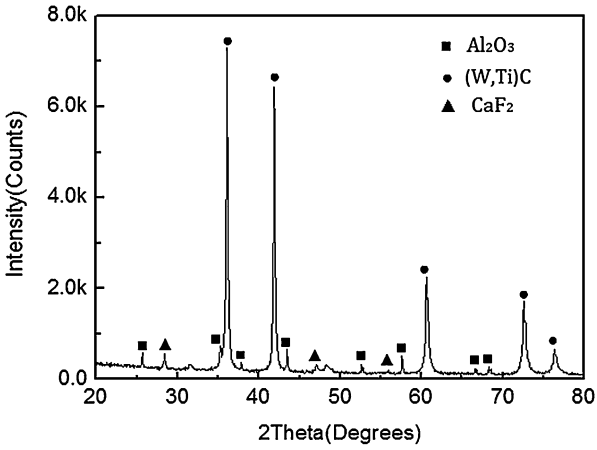

Fig. 8.4 XRD pattern of surface layer of Al_2O_3/(W,Ti)C/CaF_2 graded composite

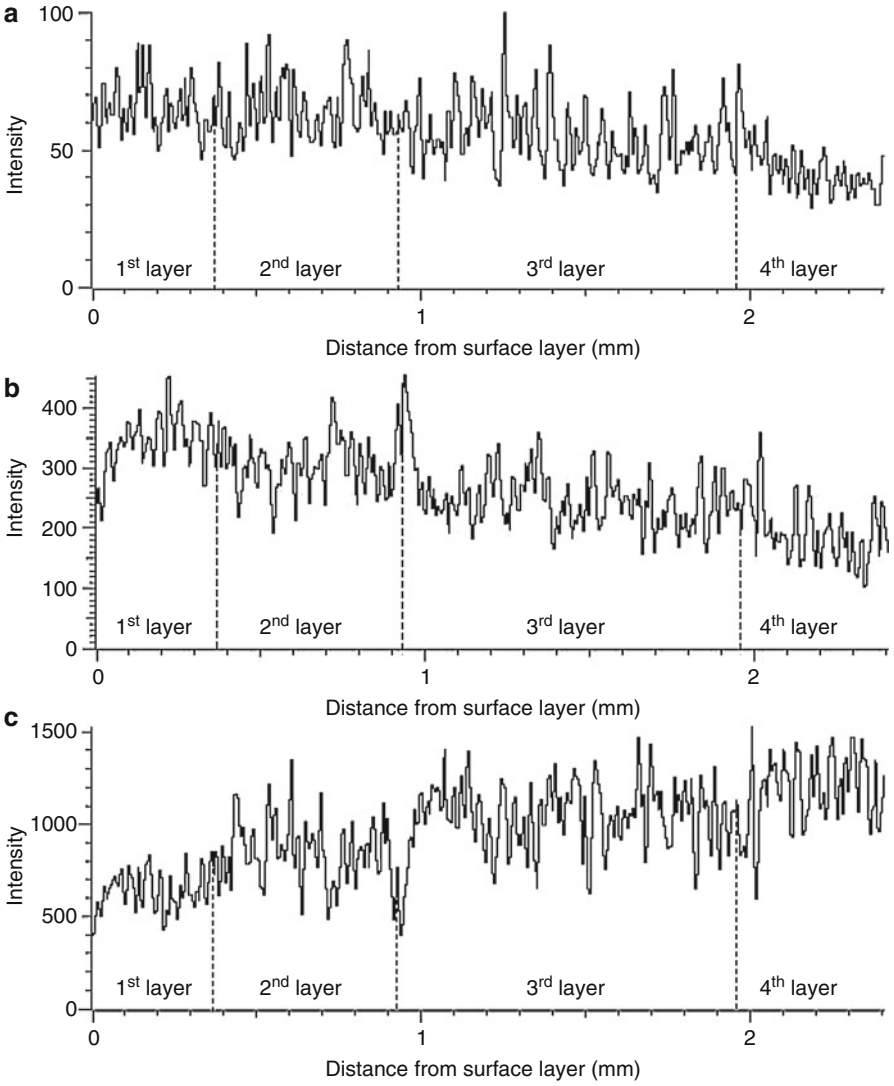

Fig. 8.5 Line scanning patterns for elemental distributions along the compositional gradient direction: (**a**) Ca element, (**b**) Ti element, and (**c**) Al element

Elemental gradient distributions from a surface layer (first layer) to the middle layer (fourth layer) are shown in Fig. 8.5. It can be seen that the concentrations of Ca and Ti elements decrease from the surface layer to the middle layer in the graded composite, whereas the Al concentration follows the opposite trend. It is indicated that the graded distributions of Al_2O_3, (W,Ti)C, and CaF_2 conform to the design scheme shown in Table 8.2. It should be noticed that a small amount of elemental Ca is detected in the middle layer of the material where no CaF_2 was added. The

Table 8.3 Mechanical properties of the self-lubricating ceramic composites

Specimen	Flexural strength (MPa)	Vickers hardness (GPa)	Fracture toughness ($MPa \cdot m^{1/2}$)
Graded composite	769±22[a]	15.36 ± 0.3[b]	4.02 ± 0.2[b]
Homogeneous composite	617 ± 31	12.89 ± 0.5	3.81 ± 0.3

[a]The testing forces were loaded perpendicularly with respect to the layers
[b]The data were from measurements taken on the surface layers

concentration of elemental Ca sharply decreases from the boundary of the fourth layer and the third layer to the interior of the fourth layer. This result could be attributed to the melting point of CaF_2, which is lower than the sintering temperature. Some CaF_2 may have melted during the sintering process and diffused into the middle layer from the adjacent layers.

The mechanical properties of Al_2O_3/(W,Ti)C/CaF_2 graded self-lubricating ceramic composite and the homogeneous composite are listed in Table 8.3. The flexural strength, Vickers hardness, and fracture toughness of the Al_2O_3/(W,Ti)C/CaF_2 graded composite are respectively 25%, 19%, and 6% higher than those of the Al_2O_3/(W,Ti)C/CaF_2 homogeneous composite. The significant improvement in the mechanical properties can be attributed to the two design criteria. Firstly, the decreasing gradient of the CaF_2 content from the surface layers to the middle layer of the graded composite can ensure excellent self-lubricating properties in the surface layers because of its relatively high CaF_2 content, and improve the flexural strength of the whole material due to substantially higher flexural strength of the middle layer where no CaF_2 had been added. Secondly, residual compressive stresses in the surface layers were caused by the mismatched thermal coefficients of expansion between adjacent layers. The presence of these stresses can effectively improve the mechanical properties of the surface layers, especially the fracture toughness and hardness [11].

The thermal residual stresses were calculated by the indentation method [12]. The indentation was produced by a Vickers indenter on central line of each layer of a cross section of the composite, using a load of 49 N. The indents were aligned in the way that their diagonals and possible radial cracks were parallel and perpendicular to the graded layers. As shown in Fig. 8.6a, the indentation cracks that are perpendicular to the layers are clearly shorter and narrower than those parallel to the layers, which indicates the presence of compressive stresses in the surface layers. It can be seen from Fig. 8.6b that the exterior layers are subjected to compressive stresses while tensile stresses are found in the interior layers. The profile of residual stresses satisfactorily conforms to the design objective.

The dry friction and wear test took pin-on-disk type and was carried out on a MMW-1A multipurpose friction and wear testing machine. The pin specimen (10 mm × 10 mm × 5 mm, Ra 0.1 μm) was made of the self-lubricating ceramic composites by cutting, grinding, and polishing. The disk was a hardened 45# carbon steel ring (Φ54mm × Φ38mm × 10 mm, HRC 45, Ra 0.08 μm). The pin and disk were ultrasonically cleaned for 10 min in acetone and then completely dried in a

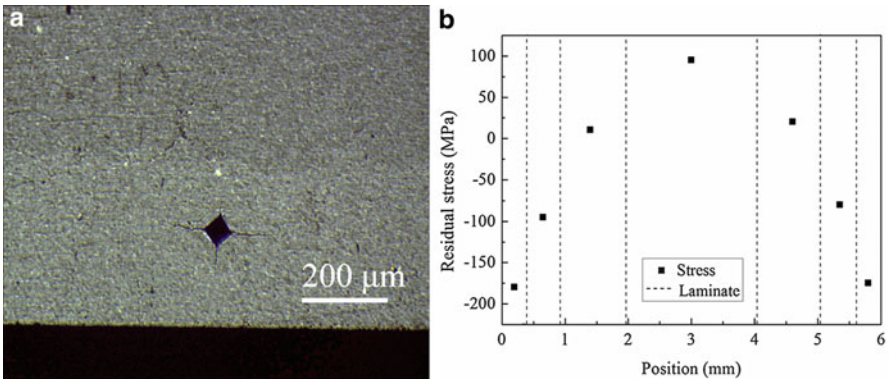

Fig. 8.6 (**a**) Optical micrograph of an indentation on the surface layer, and (**b**) profile of residual stresses measured by the indentation method

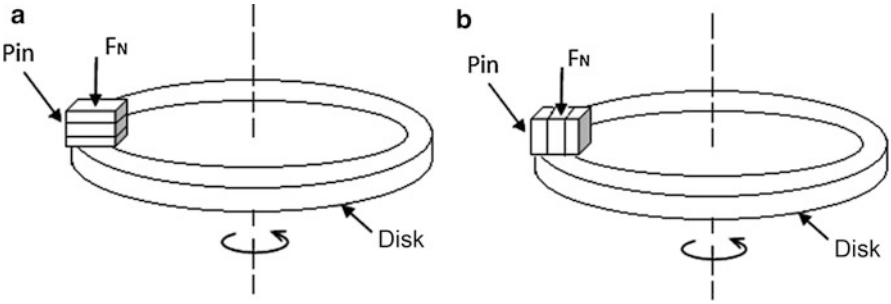

Fig. 8.7 Schematic diagrams of the testing device and clamping mode of pin specimen

vacuum drying oven. The schematic diagrams of the friction and wear testing device and clamping mode of pin specimen are shown in Fig. 8.7. During the dry friction and wear test, the pin specimen of Al_2O_3/(W,Ti)C/CaF_2 graded composite was clamped in the way shown as Fig. 8.7a and was sliding on the disk with a rotational speed of 100–300 r/min under a normal load of 100 N.

The friction coefficient μ of the ceramic composite was calculated by the formula:

$$\mu = F/P = M/(\mathrm{R} \cdot P) \tag{8.5}$$

where F is the fiction force (N); P is the normal load (N); M is the friction torque (N·m); R is intermediate radius of the steel ring (m). The friction coefficient was acquired directly from the friction and wear machine.

The wear rate W (mm^3/N·m) of the ceramic composite was calculated by the formula:

$$W = V/(L \cdot P) = m/(2\pi \cdot \mathrm{R} \cdot n \cdot t \cdot \rho \cdot P) \tag{8.6}$$

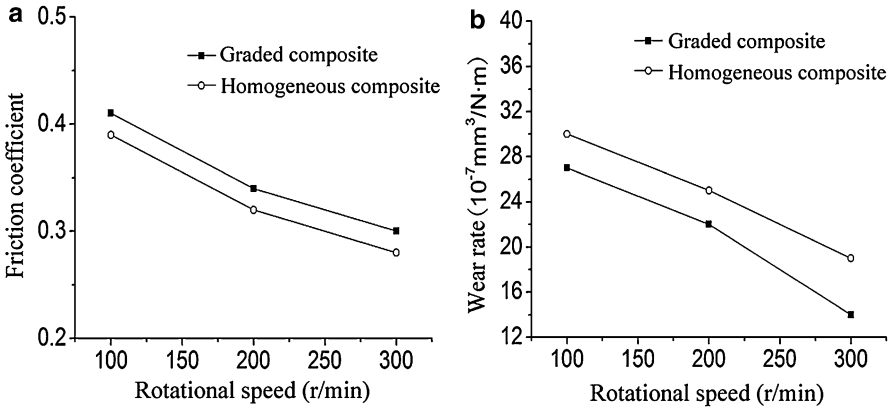

Fig. 8.8 Effect of rotational speed on (**a**) friction coefficient and (**b**) wear rate

where V is the volume loss (mm^3); L is the sliding distance (m); m is the mass loss (g); n is the rotational speed (r/min); t is the friction duration (min); ρ is the density (g/mm^3) and was measured by Archimedes method.

As shown in Fig. 8.8a, the friction coefficient of the two ceramic composites decreases with the increase of rotational speed from 100 r/min to 300 r/min. It is indicated that their antifriction property at relatively high speed is better than that at lower speed. It can also be seen that the fiction coefficient of Al_2O_3/(W,Ti)C/CaF_2 graded ceramic composite is slightly higher than that of the homogeneous one. The homogeneous ceramic composite and the surface layer of the graded ceramic composite were made from the same combined powders. They have the same CaF_2 content and other constituent content. Thus the antifriction property of Al_2O_3/(W,Ti)C/CaF_2 graded ceramic composite is comparable to that of the homogeneous one. As shown in Fig. 8.8b, the wear rate of the two ceramic composites decreases as the rotational speed increases from 100 r/min to 300 r/min. Besides, the wear rate of Al_2O_3/(W,Ti)C/CaF_2 graded ceramic composite is lower than that of Al_2O_3/(W,Ti)C/CaF_2 homogeneous composite. It means that the graded composite has better antiwear property than the homogeneous composite. According to the research of Evans et al. [5], the improvement in antiwear property should be attributed to the enhancement of mechanical properties of the graded ceramic composite, which was caused by the residual compressive stresses existing in the surface layer.

The pin specimen of the graded self-lubricating ceramic composite was clamped in the way shown as Fig. 8.7b. The cross section was used as the rubbing surface to make all layers sliding against the disk at the same time. The effect of CaF_2 content on the wear property of the ceramic composite was analyzed by observing the wear morphologies of graded layers with different composition. Figure 8.9 shows wear morphologies of graded layers with different composition under the normal load of 100 N and rotational speed of 200 r/min. It is shown that the worn surface of the fourth layer, where no CaF_2 was added, is rough and abounds with furrow-like

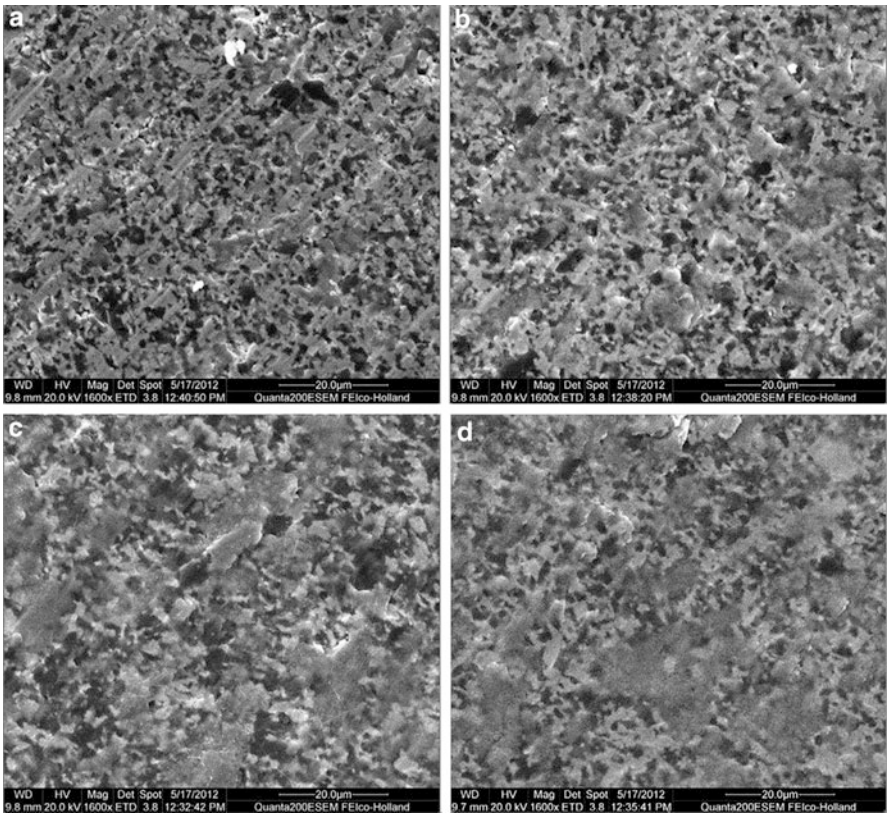

Fig. 8.9 SEM micrographs of wear morphologies of different layers: (**a**) 4th layer with 0 Vol.% CaF_2, (**b**) 3rd layer with 3.3 Vol.% CaF_2, (**c**) 2nd layer with 6.7 Vol.% CaF_2, (**d**) 1st layer with 10 Vol.% CaF_2

scratches, which is a typical sign of abrasive wear. With the increase of CaF_2 content, tribofilm with increasing coverage area was formed and abrasive wear was alleviated layer by layer. It indicates that the CaF_2 solid lubricant was released and smeared on the worn surfaces, because CaF_2 has planes of perfect crystal cleavage in its crystal structure suggesting low-shear strength [13]. Relatively complete tribofilm was formed on the wear surface of the surface layer containing 10Vol.% CaF_2. The tribofilm played a major role in antifriction and wear resistance.

8.3 Self-Lubricating Ceramic Composites with Metal Coated Solid Lubricants

Self-lubricating ceramic composites with the addition of metal coated solid lubricants were proposed in terms of microstructural modification to the traditional self-lubricating ceramic composites. Metal coated solid lubricants are composite

Table 8.4 Composition and parameters of the electroless nickel plating bath

Role in the bath	Chemical	Parameter
Main salt	Nickel sulfate ($NiSO_4 \cdot 6H_2O$)	25 g/L
Reducing agent	Sodium hypophosphite ($NaH_2PO_2 \cdot H_2O$)	25 g/L
Complexing agent	Tri-sodium citrate ($C_6H_5Na_3O_7 \cdot 2H_2O$)	50 g/L
Buffering agent	Ammonium chloride (NH_4Cl)	30 g/L
pH adjuster	Aqueous ammonia ($NH_3 \cdot H_2O$)	Proper amount
pH of solution		9.5–10.0
Plating temperature		45–50 °C
Loading ratio		2–10 g/L

powders with a solid lubricant core and metallic shell. There are many methods to synthesize core-shell composite powders with metallic shell, such as precipitation [14], chemical vapor deposition [15], electroplating [16], electroless plating [17], displacement plating [18], thermo-chemistry co-reduction [19], and gas suspension spray coating [20]. Among these methods, electroless plating has been recognized as one of the most convenient and effective techniques [21]. It is an autocatalytic chemical reduction process in which the reducing agent is oxidized and metallic ions are reduced and then deposited on the substrate surface.

In the study, metal coated solid lubricant powders were firstly prepared by ultrasonic assisted electroless plating process, and then the as-prepared coated powders were mixed with ceramic matrix powders to prepare self-lubricating ceramic composites by hot pressing.

Al_2O_3/(W,Ti)C, CaF_2, and Ni were chosen to be the matrix material, solid lubricant, and metal for coating, respectively. The starting powders were commercially available α-Al_2O_3, (W,Ti)C, and CaF_2 with average particle size of 0.5 μm, 2.5 μm, and 5 μm, respectively. Before electroless nickel plating process, the raw CaF_2 powders were cleaned, coarsened, sensitized, and activated [9]. After that, the CaF_2 powders were dispersed in distilled water and then poured into an electroless nickel plating bath with ultrasonic agitation. The composition and parameters of the plating bath are listed in Table 8.4 [9]. The overall reaction in the electroless plating can be expressed as follows [22]:

$$2Ni^{2+} + 8H_2PO_2^- + 2H_2O \rightarrow 6H_2PO_3^- + 2H^+ + 3H_2 \uparrow + 2P + 2Ni \qquad (8.7)$$

Because $NaH_2PO_2 \cdot H_2O$ was used as reductant in the plating bath, phosphorus element was electroless co-deposited with nickel atoms on CaF_2 powders to form core-shell structure. After electroless plating, the nickel coated CaF_2 powders (CaF_2@Ni) were rinsed with distilled water for several times and then dried in a vacuum oven at 100–110 °C for 8–10 h.

Figure 8.10 shows SEM micrographs of pristine CaF_2 powders and CaF_2@Ni powders with different CaF_2 loading ratios. It can be seen from Fig. 8.10a that the pristine CaF_2 powders have irregular and polyhedral shape with clean and smooth

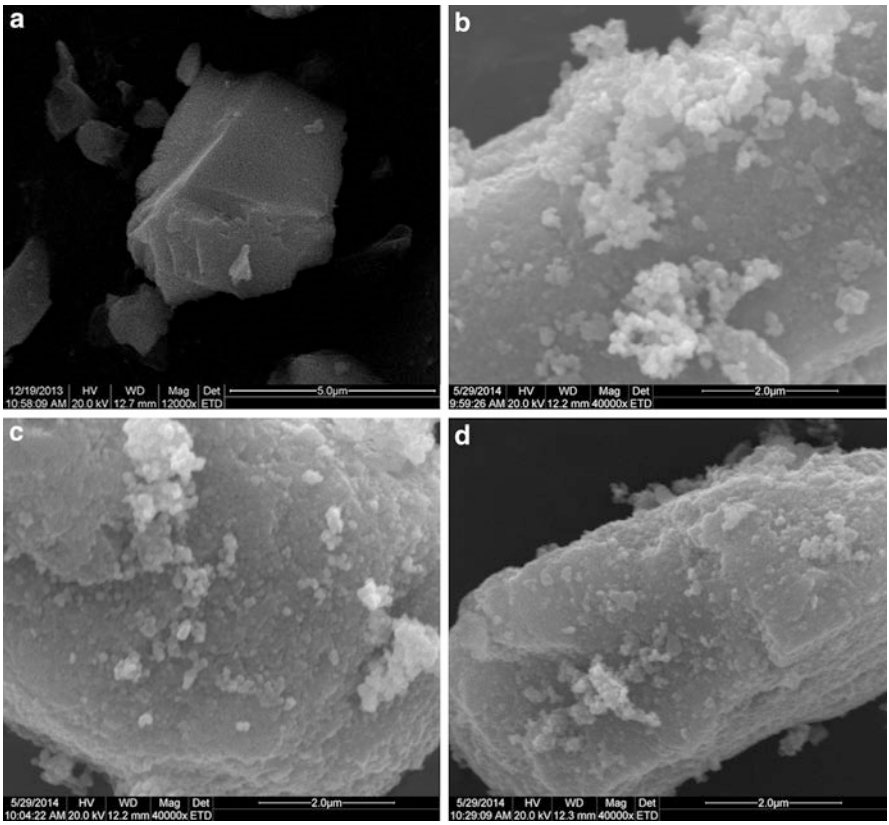

Fig. 8.10 SEM micrographs of (**a**) pristine CaF_2 powders and CaF_2@Ni powders with different CaF_2 loading ratios: (**b**) 2 g/L, (**c**) 5 g/L, (**d**) 10 g/L

surfaces. By contrast, the CaF_2@Ni powders exhibit coarse surfaces with regular nanometric spheres, as shown in Fig. 8.10b–d. When CaF_2 loading ratio is 2 g/L, the nickel coating is complete but has a lot of free Ni aggregates. When CaF_2 loading ratio is 10 g/L, the nickel coating is incompact and incomplete. The nickel coating with CaF_2 loading ratio of 5 g/L is uniform, compact, and complete. Therefore, CaF_2@Ni powders prepared when CaF_2 loading ratio was 5 g/L were used to prepare Al_2O_3/(W,Ti)C/CaF_2@Ni ceramic composite.

Figure 8.11 shows XRD pattern of CaF_2@Ni composite powders when CaF_2 loading ratio of electroless plating was 5 g/L. Besides sharp diffraction peaks belonging to CaF_2, noncrystalline background appears and there is a hillock-like peak (shown in dashed frame) near $2\theta = 45°$. EDS was used to further confirm the coating composition, as shown in Fig. 8.12. It is obviously seen that Ni and P peaks appear at the EDS spectrum besides Ca and F peaks. The XRD and EDS analysis evidently confirm that CaF_2 powders were covered by amorphous Ni-P alloy.

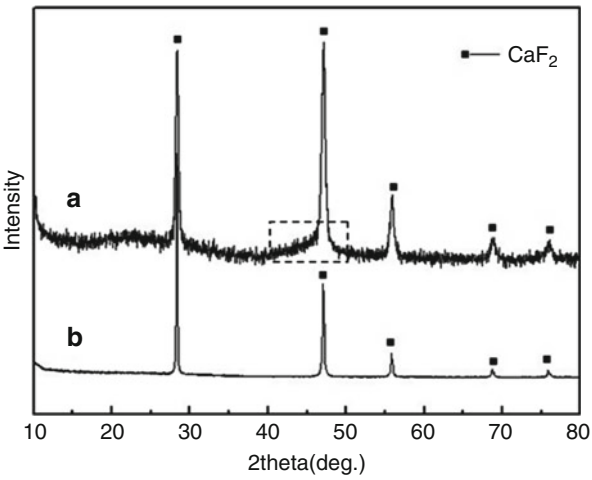

Fig. 8.11 XRD patterns of (**a**) CaF_2@Ni composite powders and (**b**) pristine CaF_2 powders

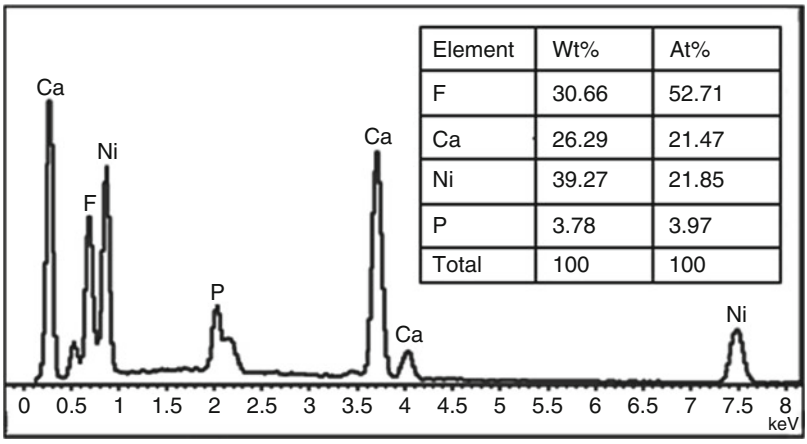

Element	Wt%	At%
F	30.66	52.71
Ca	26.29	21.47
Ni	39.27	21.85
P	3.78	3.97
Total	100	100

Fig. 8.12 EDS spectrum of CaF_2@Ni composite powders

The as-prepared CaF_2@Ni powders were mixed with the raw α-Al_2O_3 and (W,Ti)C powders (α-Al_2O_3:(W,Ti)C = 55:45, v/v) and hot pressed to produce Al_2O_3/(W,Ti)C/CaF_2@Ni ceramic composite containing 10 vol.% CaF_2@Ni powders. The detailed preparation process and measurement method of mechanical properties were described in [9]. An Al_2O_3/(W,Ti)C/CaF_2 ceramic composite with 10 vol.% uncoated CaF_2 was also prepared by using the same technical process.

Figure 8.13 shows SEM micrographs of the polished surfaces of the two ceramic composites. The light gray phase is identified by EDS to be (W,Ti)C and CaF_2, and the deep gray phase is Al_2O_3. It can be seen that the (W,Ti)C phase of Al_2O_3/(W,Ti)C/CaF_2@Ni composite is uniformly distributed in the Al_2O_3 matrix and has smoother grains than Al_2O_3/(W,Ti)C/CaF_2 composite. It is deduced that the

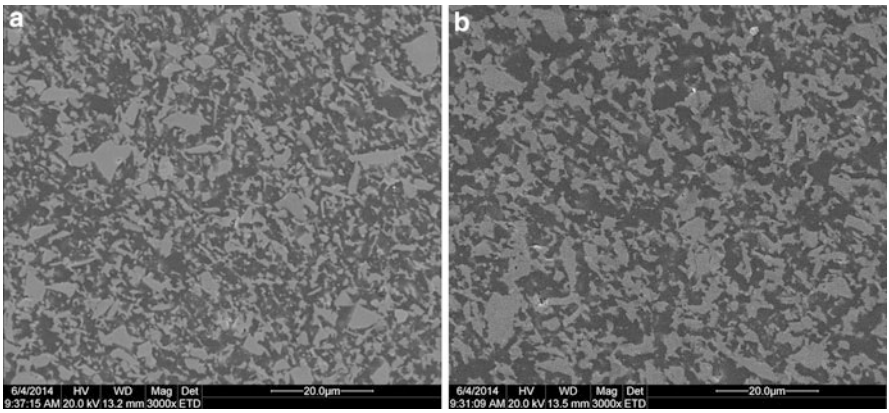

Fig. 8.13 SEM micrographs of polished surfaces: (**a**) Al_2O_3/(W,Ti)C/CaF_2 and (**b**) Al_2O_3/(W,Ti)C/CaF@Ni.

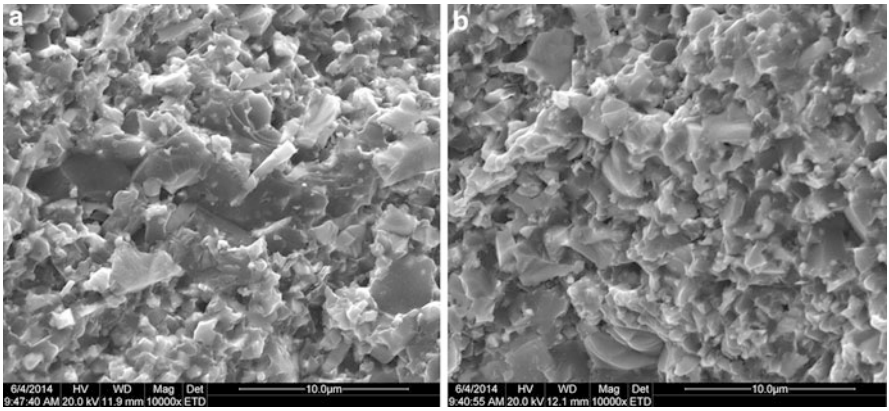

Fig. 8.14 SEM micrographs of fracture surfaces: (**a**) Al_2O_3/(W,Ti)C/CaF_2 and (**b**) Al_2O_3/(W,Ti)C/CaF_2@Ni

pointedness of (W,Ti)C in Al_2O_3/(W,Ti)C/CaF_2@Ni composite fused during the sintering process due to the addition of CaF_2@Ni powders.

Figure 8.14 presents SEM micrographs of the fracture surface of the two ceramic composites. The microstructure of Al_2O_3/(W,Ti)C/CaF_2 composite is not so homogeneous and some grains with abnormal growth can be seen. By contrast, the microstructure of Al_2O_3/(W,Ti)C/CaF_2@Ni composite is compact and the grain size of each phase is uniform. The addition of CaF_2@Ni powders leads to the improvement in microstructure. For one thing, adding the coated powders enhanced dispersity of the solid lubricants in the ceramic composite. For another, the nickel was in fluid phase at the sintering temperature and played a role in promoting densification and preventing grains from abnormally growing. Furthermore, fracture modes of the both ceramic composites are mixed transgranular fracture and intergranular fracture.

The measured flexural strength of the Al_2O_3/(W,Ti)C/CaF_2@Ni composite was 582 ± 27 MPa, which is 15% higher than that of the Al_2O_3/(W,Ti)C/CaF_2 composite (506 ± 21 MPa). The Vickers hardness of the Al_2O_3/(W,Ti)C/CaF_2@Ni composite was 14.1 ± 0.4 GPa, which was increased by 5% compared to that of the Al_2O_3/(W,Ti)C/CaF_2 composite (13.4 ± 0.3 GPa). The fracture toughness measured on the surface layers of the Al_2O_3/(W,Ti)C/CaF_2@Ni composite was 4.3 ± 0.3 MPa·$m^{1/2}$, which is 19% higher than that of the Al_2O_3/(W,Ti)C/CaF_2 composite (3.6 ± 0.2 MPa·$m^{1/2}$). The enhancement of the mechanical properties can be attributed to two reasons: firstly, the inhomogeneous distribution of a second phase and abnormally grown grains can act as the fracture origin and then do harm to mechanical properties [23], so the enhanced flexural strength and hardness of Al_2O_3/(W,Ti)C/CaF_2@Ni composite may be caused by its more homogeneous microstructure refined by adding CaF_2@Ni powders. Secondly, ceramic materials can be toughened by incorporating ductile metal particles in terms of sintering metal coated ceramic powders [24, 25]. The main toughening mechanisms are the bridging effect and the deflection of cracks by the metal particles. So the addition of CaF_2@Ni powders should account for the notable fracture toughness improvement of Al_2O_3/(W,Ti)C/CaF_2@Ni composite.

The dry friction and wear test took pin-on-disk type and was carried out on the MMW-1A multipurpose friction and wear testing machine. The pin specimen (10 mm × 10 mm × 5 mm, Ra 0.1 μm) was made of the self-lubricating ceramic composites by cutting, grinding, and polishing. The disk was a hardened 45# carbon steel ring (Φ54mm × Φ38mm × 10 mm, HRC 45, Ra 0.08 μm). The pin and disk were ultrasonically cleaned for 10 min in acetone and then completely dried in a vacuum drying oven. During the dry friction and wear test, the pin specimen was sliding on the disk with a rotational speed of 100–400 r/min under a normal load of 20 N.

The effect of the rotational speed on the friction coefficient is illustrated in Fig. 8.15a. It can be seen that with the increase of rotational speed from 100 r/min to 400 r/min, the friction coefficient of the two composites shows a downward trend. In addition, the friction coefficient of Al_2O_3/(W,Ti)C/CaF_2@Ni composite is smaller than that of Al_2O_3/(W,Ti)C/CaF_2 composite at each rotational speed. This phenomenon can be attributed to the different addition methods of CaF_2. For Al_2O_3/(W,Ti)C/CaF_2 composite, a chemical reaction between CaF_2 and Al_2O_3 may occur during the sintering process [26]:

$$3CaF_2(s) + Al_2O_3(s) \rightarrow 3CaO(s) + 2AlF_3(g) \tag{8.8}$$

The reaction results in loss of some CaF_2 and weakens the self-lubricating property of the ceramic composite. For Al_2O_3/(W,Ti)C/CaF_2@Ni composite, the metal shell of the CaF_2@Ni powders can prevent or reduce the reaction between CaF_2 and Al_2O_3. Thus Al_2O_3/(W,Ti)C/CaF_2@Ni composite exhibits better anti-friction property than Al_2O_3/(W,Ti)C/CaF_2 composite.

Figure 8.15b illustrates the effect of the rotational speed on the wear rate of the two composites. Firstly, the wear rate of the two composites decreases as the rotational speed increases from 100 r/min to 400 r/min. Secondly, the wear rate of Al_2O_3/(W,Ti)C/CaF_2@Ni composite is lower than that of Al_2O_3/(W,Ti)C/CaF_2 composite. It

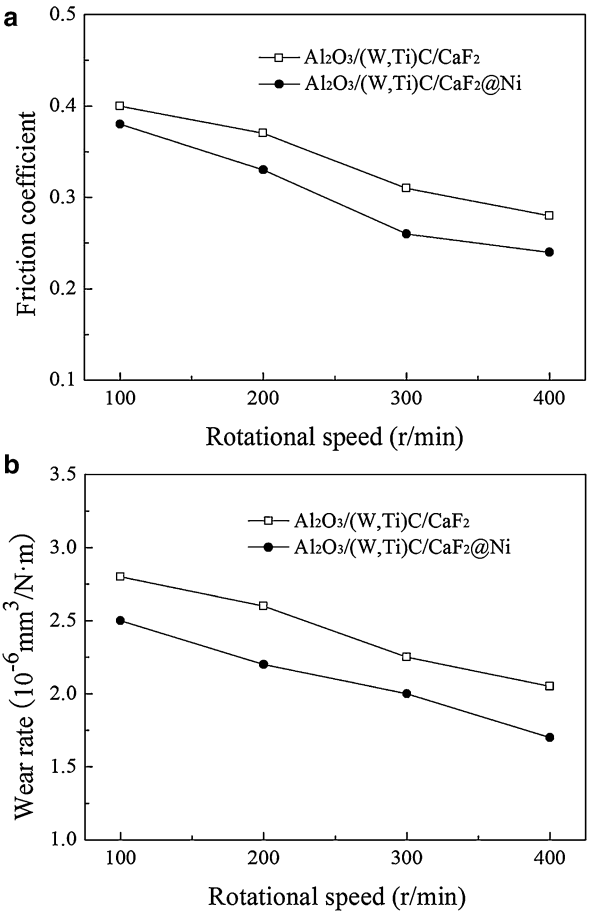

Fig. 8.15 Effect of rotational speed on (**a**) friction coefficient and (**b**) wear rate

indicates that the antiwear property of the composite with the addition of CaF_2@Ni powders is superior to that of the composite with the addition of pristine CaF_2 powders. Evans et al. reported that the wear rate of ceramic material is inversely proportional to the product of its fracture toughness and hardness, i.e., $K_{IC}^{3/4}H^{1/2}$ [5]. Therefore, the better antiwear property of Al_2O_3/(W,Ti)C/CaF_2@Ni composite can be ascribed to the higher mechanical properties especially the hardness and fracture toughness.

The worn surfaces of the two composites under the rotational speed of 200 r/min are presented in Fig. 8.16a and c, respectively. It can be seen that the worn surface of Al_2O_3/(W,Ti)C/CaF_2 composite is rougher than that of Al_2O_3/(W,Ti)C/CaF_2@Ni composite, which verifies the wear resistance of the latter is higher than the former. In addition, EDS analysis reveals that more Ca and less Fe exist on the worn surface of Al_2O_3/(W,Ti)C/CaF_2@Ni composite in comparison to Al_2O_3/(W,Ti)C/CaF_2 composite, as shown in Fig. 8.16b and d. It is indicated that the ceramic composite with

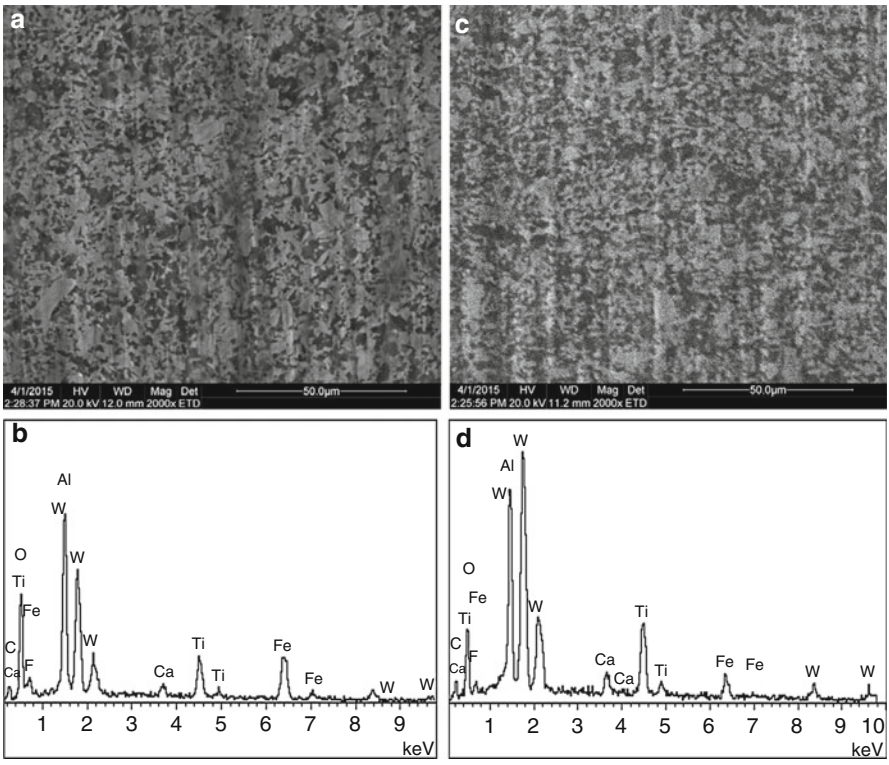

Fig. 8.16 (**a**) SEM micrograph and (**b**) EDS analysis of worn surface of Al_2O_3/(W,Ti)C/CaF_2; (**c**) SEM micrograph and (**d**) EDS analysis on worn surface of Al_2O_3/(W,Ti)C/CaF_2@Ni.

the addition of CaF_2@Ni powders has better antiadhesive property than the ceramic composite with the addition of pristine CaF_2 powders.

8.4 Summary

Aiming at the difficult problem that the traditional self-lubricating ceramic composites are not available to possess rational combination of antifriction and antiwear properties, two new types of self-lubricating ceramic composites were developed in recent years. They modified the traditional self-lubricating ceramic composites at macroscopic and microscopic levels, respectively.

Al_2O_3/(W,Ti)C/CaF_2 graded self-lubricating ceramic composite was developed in terms of macrostructural modification. The microstructures changed layer by layer, which agreed with the gradient variation of the components. The exterior layers were subjected to compressive stresses and the interior layers were subjected to tensile stresses. The flexural strength, Vickers hardness, and fracture toughness of the Al_2O_3/(W,Ti)C/CaF_2 graded composite were respectively 25%, 19% and 6% higher than those of the homogeneous Al_2O_3/(W,Ti)C/CaF_2 composite. The dry friction and

wear test showed that the graded self-lubricating ceramic composite had comparable antifriction properties and superior antiwear properties to the homogeneous composite. The evident improvement in the mechanical and tribological properties can be attributed to the fulfillment of the two design criteria. For one thing, the gradually decreasing distribution of CaF_2 from the composite's surface layers to middle layer ensured good self-lubricating property of the surface layers and enhanced the flexural strength of the graded composite. For another, the existing residual compressive stresses increased hardness, fracture toughness, and antiwear properties of the surface layers of the graded composite.

Al_2O_3/(W,Ti)C/CaF_2@Ni self-lubricating ceramic composite with the addition of metal coated solid lubricants was developed in terms of microstructural modification. As compared with the Al_2O_3/(W,Ti)C/CaF_2 composite, the microstructure of Al_2O_3/(W,Ti)C/CaF_2@Ni composite was more uniform. The flexural strength, Vickers hardness, and fracture toughness were increased by about 15%, 5%, and 19%, respectively. The dry friction and wear test showed that Al_2O_3/(W,Ti)C/CaF_2@Ni composite had obviously better antifriction and antiwear properties than Al_2O_3/(W,Ti)C/CaF_2 composite. The addition of CaF_2@Ni powders led to the improvement in the microstructure, mechanical properties, and tribological behaviors. Firstly, the nickel shell of CaF_2@Ni powders promoted dispersity of CaF_2 in the ceramic composite and protected CaF_2 from reacting with the Al_2O_3 matrix, which enhanced antifriction property. Secondly, the nickel shell promoted the ceramic composite's densification, prevented grains from abnormally growing, and toughened the ceramic composite, which improved the microstructure, mechanical properties, and antiwear property.

Acknowledgments This research work was supported by the National Natural Science Foundation of China, Grant No. 51075248 and Grant No. 51575285.

References

1. Reis, P., Filho, V., Davim, J.P., Xu, X., Ferreira, J.M.F.: Wear behavior on advanced structural ceramics: α-sialon matrix reinforced with b-sialon fibers. Mater. Design. **26**, 417–423 (2005)
2. Deng, J., Cao, T.: Self-lubricating mechanisms via the in situ formed tribofilm of sintered ceramics with CaF_2 additions when sliding against hardened steel. Int. J. Refract. Met. Hard Mater. **25**, 189–197 (2007)
3. Carrapichano, J.M., Gomes, J.R., Silva, R.F.: Tribological behaviour of Si_3N_4-BN ceramic materials for dry sliding applications. Wear. **253**, 1070–1076 (2002)
4. Deng, J., Cao, T., Ding, Z., Liu, J., Sun, J., Zhao, J.: Tribological behaviors of hot-pressed Al_2O_3/TiC ceramic composites with the additions of CaF_2 solid lubricants. J. Eur. Ceram. Soc. **26**, 1317–1323 (2006)
5. Evans, A.G., Wilshaw, T.R.: Quasi-static solid particle damage in brittle solids – I. Observations analysis and implications. Acta Metall. **24**, 939–956 (1976)
6. Wu, G., Xu, C., Zhang, Y., Yi, M.: State of the art of graded self-lubricating ceramic cutting tool materials. Appl. Mech. Mater. **66–68**, 1598–1604 (2011)
7. Xu, C.H., Wu, G.Y., Xiao, G.C., Fang, B.: Al_2O_3/(W,Ti)C/CaF_2 multi-component graded self-lubricating ceramic cutting tool material. Int. J. Refract. Met. Hard Mater. **45**, 125–129 (2014)
8. Xu, C., Wu, G., Zhang, Y., Yi, M., Xiao, G., Fang, B.: Development of multicomponent graded self-lubricating ceramic cutting tool materials. J. Mech. Eng. **50**(7), 94–101 (2014)

9. Wu, G., Xu, C., Xiao, G., Yi, M., Chen, Z., Xu, L.: Self-lubricating ceramic cutting tool material with the addition of nickel coated CaF_2 solid lubricant powders. Int. J. Refract. Met. Hard Mater. **56**, 51–58 (2016)
10. Ai, X., Zhao, J., Huang, C., Zhang, J.: Development of an advanced ceramic tool material – functionally gradient cutting ceramics. Mater. Sci. Eng. A. **248**(1–2), 125–131 (1998)
11. Mehrali, M., Wakily, H., Metselaar, I.H.S.C.: Residual stress and mechanical properties of Al_2O_3/ZrO_2 functionally graded material prepared by EPD from 2-butanone based suspension. Adv. Appl. Ceram. **110**, 35–40 (2011)
12. Hvizdoš, P., Jonsson, D., Anglada, M., Anné, G., Biest, O.V.D.: Mechanical properties and thermal shock behaviour of an alumina/zirconia functionally graded material prepared by electrophoretic deposition. J. Eur. Ceram. Soc. **27**, 1365–1371 (2007)
13. Shuaib, M., Davies, T.J.: Wear behaviour of a REFEL SiC containing fluorides up to 900 °C. Wear. **249**, 20–30 (2001)
14. Li, G., Huang, X., Guo, J.: Fabrication of Ni-coated Al_2O_3 powders by the heterogeneous precipitation method. Mater. Res. Bull. **36**, 1307–1315 (2001)
15. Chen, C.-C., Chen, S.-W.: Nickel and copper deposition on Al_2O_3 and SiC particulates by using the chemical vapour deposition-fluidized bed reactor technique. J. Mater. Sci. **32**, 4429–4435 (1997)
16. Chen, L., Yu, G., Chu, Y., Zhang, J., Hu, B., Zhang, X.: Effect of three types of surfactants on fabrication of Cu-coated graphite powders. Adv. Powder Technol. **24**, 281–287 (2013)
17. Amirjan, M., Zangeneh Madar, K., Parvin, N.: Evaluation of microstructure and contiguity of W/Cu composites prepared by coated tungsten powders. Int. J. Refract. Met. Hard Mater. **27**, 729–733 (2009)
18. Zhang, R., Gao, L., Guo, J.: Preparation and characterization of coated nanoscale Cu/SiCp composite particles. Ceram. Int. **30**, 401–404 (2004)
19. Li, J., Chen, W., Tao, W., Shao, F., Ding, B.: Nano-composite powder of tungsten coated copper produced by thermo-chemistry co-reduction. Rare Met. Mater. Eng. **41**, 2091–2094 (2012)
20. Choi, W.C., Byun, D., Lee, J.K., Cho, B.W.: Electrochemical characteristics of silver- and nickel-coated synthetic graphite prepared by a gas suspension spray coating method for the anode of lithium secondary batteries. Electrochim. Acta. **50**, 523–529 (2004)
21. Xu, X., Cui, Z.D., Zhu, S.L., Liang, Y.Q., Yang, X.J.: Preparation of nickel-coated graphite by electroless plating under mechanical or ultrasonic agitation. Surf. Coating Technol. **240**, 425–431 (2014)
22. Hu, B., Sun, R., Yu, G., Liu, L., Xie, Z., He, X., et al.: Effect of bath pH and stabilizer on electroless nickel plating of magnesium alloys. Surf. Coating Technol. **228**, 84–91 (2013)
23. Oh, S.-T., Sando, M., Niihara, K.: Mechanical and magnetic properties of Ni-Co dispersed Al_2O_3 nanocomposites. J. Mater. Sci. **36**, 1817–1821 (2001)
24. Mao, D.S., Liu, X.H., Li, J., Guo, S.Y., Zhang, X.B., Mao, Z.Y.: A fine cobalt-toughened Al_2O_3-TiC ceramic and its wear resistance. J. Mater. Sci. **33**, 5677–5682 (1998)
25. Zhu, L., Luo, L., Li, J., Wu, Y.: The influence of powder characteristics on mechanical properties of Al_2O_3-TiC-Co ceramic materials prepared by Co-coated Al_2O_3/TiC powders. Int. J. Refract. Met. Hard Mater. **34**, 61–65 (2012)
26. Wang, Q., Ge, Y., Cui, W., Chen, K., Ferreira, J.M.F., Xie, Z.: Carbothermal synthesis of micro-scale spherical AlN granules with CaF_2 additive. J. Alloy Compd. **663**, 823–828 (2016)